# Optical-field-induced Electron Emission in a dc-Biased Nanogap

Yi Luo[†] and Peng Zhang[*]

*Department of Electrical and Computer Engineering, Michigan State University, East Lansing, Michigan 48824-1226, USA*

(Received 21 December 2021; revised 1 March 2022; accepted 21 March 2022; published 5 April 2022)

We construct an analytical formulation for nonlinear photoelectron emission in a dc-biased metallic nanovacuum gap triggered by a laser field, by exactly solving the one-dimensional time-dependent Schrödinger equation. We theoretically investigate the photoelectron energy spectra and emission current from left- and right-side surfaces of the asymmetric nanojunction with various dc biases, laser fields, and gap distances. The underlying photoemission mechanisms transitioning form multiphoton over-barrier emission to photon-assisted field tunneling, and the spatiotemporal dynamics of electron transport inside the gap are analyzed in detail. Our calculation shows applying a dc field could greatly reduce the interference oscillation in the transmission current in the nanogap, due to the shift of dominant emission away from the multiphoton over-barrier regime. Our results demonstrate that, besides the dc bias, varying the gap spacing could strongly influence the rectification on the photoelectron emission in a dc-biased metal-vacuum-metal gap. Our study provides useful guideline to the design of ultrafast nanogap-based signal rectification devices, such as photoelectron emitters and photodetectors, by choosing an optimal combination of dc bias, gap spacing, and material properties.

DOI: 10.1103/PhysRevApplied.17.044008

## I. INTRODUCTION

Optical-field-induced electron emission from nanostructures enables the control of electron dynamics on ultrashort space and time scales [1–16], due to the nanoscopic confinement of optical electric field and the resulting large field enhancement factor on the nanosurface, which makes it crucial in many research areas, such as high-resolution electron microscopy [17–20], highly coherent electron sources [21–23], tabletop laser accelerators [24], and emerging nanoelectronic devices [25–29]. Recently, laser-driven photoelectron emission in the nanoscale gap formed between two metallic tips has drawn substantial interests [30–38], due to its promising applications to surface-enhanced spectroscopies, nonlinear optics, nanophotonics, and ultrafast and highly sensitive photodetection at room temperature. Rybka *et al*. [32] reported laser-induced subfemtosecond photoelectron tunneling in a nanoscale metal-vacuum-metal gap. Higuchi *et al*. [31] explored the rectification effect of dc-biased two-metal-nanotip junction in ultrafast multiphoton photoemission. Piltan *et al*. [34] demonstrated the plasmon-enhanced photoemission in metal-vacuum nanotip array and optical tunability from geometric degree of freedom. Ludwig *et al*. [36] presented the strong dependence of dynamics of nanoscale electron transport between two metal tips on the temporal profile of driving laser pulses. Turchetti *et al*. [38] studied the impact of dc bias on photoemission from metal surfaces surrounding a nanovacuum gap.

While there have been significant theoretical efforts to study intense-field nonlinear photoexcitation and tunneling emission process in solid systems [10,39–50], these theoretical models are valid only in certain emission regimes. For example, the perturbative theory [39,40] typically uses strong field approximation, and the Floquet theory [45,47] is developed without considering the effect of dc field. Generally, numerical solutions, like solving the time-dependent density-functional theory [30,36,37,51,52] and the Schrödinger equation [38], are implemented to study the photoelectron emission in the nanogap, such as electron transfer in plasmonic nanotips [36], nanoparticle dimers [51], and bowtie nanoantennas [53]. To reveal more clearly the underlying emission physics, most recently we developed an exact analytical model for the photoelectron emission in the metal-vacuum-metal nanogap [54], where the dependence of emission properties on the laser field, gap spacing, and metal material is studied. However, it accounts only for the symmetric nanovacuum system in which the net photoemission current is physically unobservable (i.e., the time-averaged net photocurrent is zero). For asymmetric scenarios (e.g., operating under a dc bias [30,31,34,38]) that generate experimentally observable net photocurrent, there is still a lack of an exact analytical theory (or theories) that can systematically characterize

[*]pz@egr.msu.edu

[†]Present address: Department of Electrical Engineering, University of Notre Dame, Notre Dame, Indiana 46556, USA.

 

the parametric dependence of emission properties and distinctly reveal the interplay of various processes on which emission depends.

In this work, we construct an analytical model for nonlinear optical-field-triggered photoemission in a dc-biased asymmetric metal-vacuum-metal nanojunction, by exactly solving the time-dependent Schrödinger equation (TDSE). Our model is valid in various emission regimes spanning multiphoton absorption and emission, photon-assisted tunneling, optical field emission, and dc field emission. We analyze the photoelectron emission properties from both sides of the nanovacuum gap with various combinations of dc fields, laser intensities, and gap distances. Our results show that the external dc bias could greatly enhance the photoemission current and reduce the quantum-mechanical interference oscillations in the transmission current. Furthermore, the change of the gap spacing is found to strongly influence the rectification on the photoelectron emission. This may offer practical guidance to improve signal efficiency of advanced ultrafast nanogap-based photoelectron emitters and photodetectors consisting of nanotips, nanobowties, and nanoparticles, by the choice of proper combination of dc bias, gap distance, and material properties.

## II. ANALYTICAL FORMULATION

The schematic of the configuration for a metal-vacuum-metal nanogap with a dc bias under the illumination of optical field is shown in Fig. 1(a). With the external applied dc voltage $V$, the symmetry of the metal-vacuum-metal system is broken. This means that under the same illumination condition, the left and right metal-vacuum interfaces of the nanogap in Fig. 1(a) have different photoemission properties. Therefore, we analytically model photoelectron emission from left- and right-side metal-vacuum interfaces, respectively. Here, the laser field $F_1\cos(\omega t)$ is assumed to be perpendicular to the flat metal surfaces and cuts off abruptly at the surfaces, where $F_1$ is the amplitude of the laser field and $\omega$ is the angular frequency. For simplicity, the impact of image and space charges [29,55,56] is neglected in this work.

For photoemission from the left metal-vacuum interface of the gap in Fig. 1(a), electrons in the left metal with the initial energy $\varepsilon$ would see a potential barrier subjected to a positive dc electric field $F_0 = V/d\ (>0)$ and laser field $F_1\cos(\omega t)$, as shown in Fig. 1(b). Thus, the time-dependent potential energy in the left metal ($x<0$), vacuum gap ($0<x<d$), and right metal ($x\geq d$) of Fig. 1(a) reads as [10,12,54,57–59]

$$\Phi(x,t)=\begin{cases}0 & x<0\\ E_F+W-eVx/d-eF_1x\cos(\omega t) & 0\leq x<d,\\ -eV-eF_1d\cos(\omega t) & x\geq d\end{cases} \tag{1}$$

where $E_F$ and $W$ are the Fermi energy and work function of the left metal, respectively, $e$ is the elementary charge, and $V$ is the magnitude of the applied dc bias.

To obtain the electron emission probability, we solve the TDSE,

$$i\hbar\frac{\partial\psi(x,\,t)}{\partial t}=-\frac{\hbar^2}{2m_e}\frac{\partial^2\psi(x,\,t)}{\partial x^2}+\Phi(x,\,t)\psi(x,\,t), \tag{2}$$

where $\hbar$ is the reduced Planck constant, $\psi(x,\,t)$ is the electron wave function, $m_e$ is the electron mass, and $\Phi(x,\,t)$ is the potential energy given in Eq. (1).

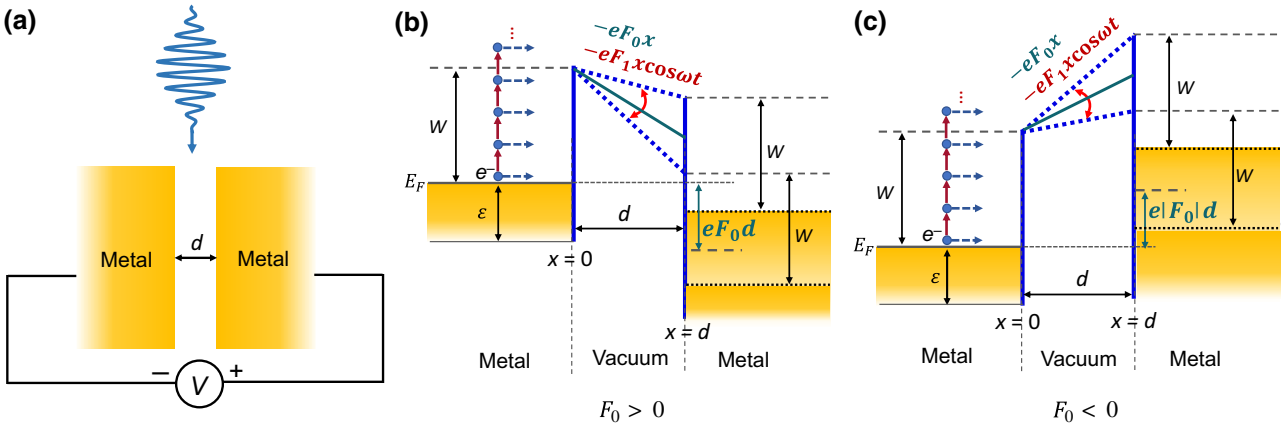


FIG. 1. (a) Schematic of the metal-vacuum-metal nanogap with a dc bias $V$ under the illumination of laser field. $d$ is the gap distance. (b) Energy diagram for photoelectron emission from the left metal-vacuum interface of the gap in (a). Electrons with initial energy $\varepsilon$ would see a potential barrier subjected to a positive dc electric field $F_0 = V/d\ (>0)$ and laser field $F_1\cos(\omega t)$. (c) Energy diagram for photoelectron emission from the right metal-vacuum interface of the gap in (a). Electrons would see a potential barrier with a negative dc electric field $F_0 = -V/d\ (<0)$ and laser field $F_1\cos(\omega t)$ with $F_1$ of opposite sign of that in (b) at any time instant for a given laser field.

For $x < 0$, the electron wave function is

$$\psi_1(x,\ t) = \exp\left(-\frac{i\varepsilon t}{\hbar} + ik_0 x\right) + \sum_{n=-\infty}^{\infty} R_{1n} \exp\left(-i\frac{\varepsilon + n\hbar\omega}{\hbar}t - ik_n x\right),\ x < 0, \tag{3}$$

which denotes the superposition of an incident plane wave with initial energy $\varepsilon$ and a set of reflected plane waves with reflection coefficient $R_{1n}$ and energies $\varepsilon + n\hbar\omega$, where the wave number $k_0 = \sqrt{2m_e\varepsilon/\hbar^2}$ and $k_n = \sqrt{2m_e(\varepsilon + n\hbar\omega)/\hbar^2}$.

For $0 \le x < d$ in the gap, the exact solution to Eq. (2) is found to be (see Appendix A for the method),

$$\psi_2(x,\ t) = \sum_{n=-\infty}^{\infty} \exp\left[-i\frac{\varepsilon + n\hbar\omega}{\hbar}t\right] \exp\left[-\frac{ie^2VF_1\sin(\omega t)}{\hbar d m_e\omega^3} + \frac{ixeF_1\sin(\omega t)}{\hbar\omega} + \frac{ie^2F_1^2\sin(2\omega t)}{8m_e\hbar\omega^3}\right] \times [T_{1n}\mathrm{Ai}(-\eta_n) + T_{2n}\mathrm{Bi}(-\eta_n)];\ 0 \le x < d, \tag{4}$$

which represents the superposition of a set of transmitted and reflected electron waves inside the gap, where

$$\eta_n = \left[\frac{E_n}{eV}d + x + \frac{eF_1\cos(\omega t)}{m_e\omega^2}\right]\left(\frac{2em_eV}{\hbar^2 d}\right)^{1/3},$$

the drift kinetic energy $E_n = \varepsilon + n\hbar\omega - E_F - W - U_p$, the ponderomotive energy $U_p = e^2F_1^2/4m_e\omega^2$, Ai and Bi are the Airy functions of the first and second kind, respectively, and $T_{1n}$ and $T_{2n}$ are the coefficients.

For $x \ge d$, an exact solution of electron wave function is

$$\psi_3(x,\ t) = \sum_{n=-\infty}^{\infty} T_{3n} \exp\left(-i\frac{\varepsilon + n\hbar\omega}{\hbar}t\right) \times \exp\left[ik_n x + i\frac{eF_1 d\sin(\omega t)}{\hbar\omega}\right],\ x \ge d, \tag{5}$$

which shows the superposition of electron plane waves transmitted into the right metal in Fig. 1(a) with energies $\varepsilon + n\hbar\omega$, due to multiphoton absorption ($n > 0$), direct tunneling ($n = 0$), and multiphoton emission ($n < 0$) [10,50], where the wave number $k_n = \sqrt{2m_e(\varepsilon + n\hbar\omega + eV)/\hbar^2}$ and $T_{3n}$ is the transmission coefficient.

The coefficients $T_{1n}$, $T_{2n}$, and $T_{3n}$ (and therefore reflection coefficient $R_{1n}$) can be calculated from boundary conditions that both the electron wave function $\psi(x,\ t)$ and its first derivative $\partial\psi(x,\ t)/\partial x$ are continuous at $x = 0$ and $x = d$ (see Appendix B for details).

The normalized transmitted current density is defined as the ratio of the transmitted probability current density over the incident probability current density, $w(\varepsilon,\ x,\ t) = J_t(\varepsilon,\ x,\ t)/J_i(\varepsilon,\ x,\ t)$, where the probability current density $J(x,\ t) = (i\hbar/2m_e)(\psi\nabla\psi^* - \psi^*\nabla\psi) = (i\hbar/2m_e)\sum_{n=-\infty}^{\infty}\sum_{l=-\infty}^{\infty}(\psi_n\nabla\psi_l^* - \psi_n^*\nabla\psi_l)$, where $\psi_n$ ($\psi_l$) is the electron wave function with eigenenergy of $\varepsilon + n\hbar\omega$ ($\varepsilon + l\hbar\omega$), which is given by the term inside the sum sign in Eq. (3) (in the left metal), Eq. (4) (inside the gap), or Eq. (5) (in the right metal). Thus, the normalized instantaneous transmitted current density in the right-side metal ($x > d$), in nondimensional quantities [10,12,54,57], $\bar{\varepsilon} = \varepsilon/W$, $\bar{\omega} = \omega\hbar/W$, $\bar{t} = tW/\hbar$, $\bar{E}_F = E_F/W$, $\bar{x} = x/\lambda_0$, $\bar{d} = d/\lambda_0$, $\lambda_0 = \sqrt{\hbar^2/2m_eW}$, $\bar{V} = eV/W$, $\bar{F}_1 = eF_1\lambda_0/W$, $\bar{U}_p = U_p/W$, and $\bar{E}_n = \bar{\varepsilon} + n\bar{\omega} - \bar{E}_F - \bar{U}_p - 1$, is found to be,

$$w(\bar{\varepsilon},\bar{t}) = \frac{1}{\sqrt{\bar{\varepsilon}}}\sum_{n=-\infty}^{\infty}\sum_{l=-\infty}^{\infty}\mathrm{Re}\{e^{i\,(l-n)\bar{\omega}\bar{t}}T_{3n}T_{3l}^*D\}, \tag{6}$$

where $D = \mathrm{e}^{\,i\left[\sqrt{\bar{\varepsilon}+n\bar{\omega}+\bar{V}} - \left(\sqrt{\bar{\varepsilon}+l\bar{\omega}+\bar{V}}\right)^*\right]\bar{x}}\left(\sqrt{\bar{\varepsilon}+l\bar{\omega}+\bar{V}}\right)^*$.

The time-averaged transmitted current density is obtained as

$$\langle w(\bar{\varepsilon})\rangle = \sum_{n=-\infty}^{\infty}\langle w_n(\bar{\varepsilon})\rangle,$$
$$\langle w_n(\bar{\varepsilon})\rangle = \mathrm{Re}\left(|T_{3n}|^2\sqrt{1 + n\bar{\omega}/\bar{\varepsilon} + \bar{V}/\bar{\varepsilon}}\right), \tag{7}$$

where $\langle w_n\rangle$ represents the time-averaged transmitted current density through $n$-photon process, with transmitted electrons of energy $\varepsilon + n\hbar\omega$.

For photoemission from right-side metal-vacuum interface of the gap in Fig. 1(a), electrons in the right metal would see a potential barrier subjected to a negative dc electric field $F_0 = -V/d$ ($< 0$) and laser field $F_1\cos(\omega t)$, as shown in Fig. 1(c). Thus, the time-dependent potential barrier in the right metal of Fig. 1(a) [$x < 0$ in Fig. 1(c)], vacuum gap ($0 < x < d$) and left metal of Fig. 1(a) [$x \ge d$ in Fig. 1(c)] is [10,12,54,57–59]

$$\Phi(x,t) = \begin{cases} 0 & x < 0 \\ E_F + W + eVx/d - eF_1x\cos(\omega t) & 0 \le x < d, \\ eV - eF_1 d\cos(\omega t) & x \ge d \end{cases} \tag{8}$$

where $E_F$ and $W$ are the Fermi energy and work function of the right metal in Fig. 1(a), respectively, and $V$ is the magnitude of the applied dc bias. Other parameters have the same definition as that in Eq. (1), with $F_1$ of opposite sign (i.e., 180° out of phase) of that in Fig. 1(b) at any time instant for a given laser field.

Solving the TDSE in Eq. (2) with the potential energy given in Eq. (8) yields the electron wave function for $x < 0$,

$$\psi_4(x,\ t) = \exp\left(-\frac{i\varepsilon t}{\hbar} + ik_0 x\right) + \sum_{n=-\infty}^{\infty} R_{2n} \exp\left(-i\frac{\varepsilon + n\hbar\omega}{\hbar}t - ik_n x\right),\ x < 0, \tag{9}$$

where the wave number $k_0 = \sqrt{2m_e\varepsilon/\hbar^2}$ and $k_n = \sqrt{2m_e(\varepsilon + n\hbar\omega)/\hbar^2}$, and $R_{2n}$ is the reflection coefficient.

For $0 \le x < d$ in the gap, the exact solution to Eq. (2) is (see Appendix A for the method),

$$\psi_5(x,\ t) = \sum_{n=-\infty}^{\infty} \exp\left[-i\frac{\varepsilon + n\hbar\omega}{\hbar}t\right] \exp\left[\frac{ie^2VF_1\sin(\omega t)}{\hbar d m_e\omega^3} + \frac{ixeF_1\sin(\omega t)}{\hbar\omega} + \frac{ie^2F_1^2\sin(2\omega t)}{8m_e\hbar\omega^3}\right] \times [T_{4n}\mathrm{Ai}(\eta_n) + T_{5n}\mathrm{Bi}(\eta_n)];\quad 0 \le x < d \tag{10}$$

representing the superposition of a set of transmitted and reflected electron waves inside the gap, where

$$\eta_n = \left[-\frac{E_n}{eV}d + x + \frac{eF_1\cos(\omega t)}{m_e\omega^2}\right]\left(\frac{2em_eV}{\hbar^2 d}\right)^{1/3},$$
$$E_n = \varepsilon + n\hbar\omega - E_F - W - U_p,$$

$U_p = e^2F_1^2/4m_e\omega^2$, and $T_{4n}$ and $T_{5n}$ are the coefficients.

For $x \ge d$, an exact solution of transmitted electron wave function is found to be

$$\psi_6(x,t) = \sum_{n=-\infty}^{\infty} T_{6n} \exp\left(-i\frac{\varepsilon + n\hbar\omega}{\hbar}t\right) \times \exp\left[ik_n x + i\frac{eF_1 d\sin(\omega t)}{\hbar\omega}\right],\ x \ge d, \tag{11}$$

where the wave number $k_n = \sqrt{2m_e(\varepsilon + n\hbar\omega - eV)/\hbar^2}$ due to $n$-photon contribution, and $T_{6n}$ is the transmission coefficient.

Similarly, the coefficients $T_{4n}$, $T_{5n}$, and $T_{6n}$ (and therefore $R_{2n}$) can be obtained from boundary conditions for continuous electron functions at $x = 0$ and $x = d$ (see Appendix B for details). The normalized instantaneous transmitted current density to the left-side metal of Fig. 1(a), defined as the ratio of the transmitted probability current density over the incident probability current density, $w(\varepsilon,\ x,\ t) = J_t(\varepsilon,\ x,\ t)/J_i(\varepsilon,\ x,\ t)$, is obtained as

$$w(\bar{\varepsilon}, \bar{t}) = \frac{1}{\sqrt{\bar{\varepsilon}}} \sum_{n=-\infty}^{\infty} \sum_{l=-\infty}^{\infty} Re\{e^{i\,(l-n)\bar{\omega}\bar{t}} T_{6n} T_{6l}^{*} D\}, \tag{12}$$

where $D = e^{i\left[\sqrt{\bar{\varepsilon}+n\bar{\omega}-\bar{V}} - \left(\sqrt{\bar{\varepsilon}+l\bar{\omega}-\bar{V}}\right)^{*}\right]\bar{x}} \left(\sqrt{\bar{\varepsilon}+l\bar{\omega}-\bar{V}}\right)^{*}$. The time-averaged transmitted current density is found to be

$$\langle w(\bar{\varepsilon})\rangle = \sum_{n=-\infty}^{\infty} \langle w_n(\bar{\varepsilon})\rangle,$$
$$\langle w_n(\bar{\varepsilon})\rangle = \mathrm{Re}\left(|T_{6n}|^2\sqrt{1 + n\bar{\omega}/\bar{\varepsilon} - \bar{V}/\bar{\varepsilon}}\right). \tag{13}$$

## III. RESULTS AND DISCUSSION

In our calculation, positive dc field ($F_0 > 0$) and negative dc field ($F_0 < 0$) denote the electron emission from left and right metal surfaces of the nanovacuum gap with the external dc voltage $V(= |F_0|d)$, respectively (cf. Fig. 1). Unless mentioned otherwise, the default value of the laser wavelength is 800 nm ($\hbar\omega = 1.55$ eV), the metals on both sides of the gap are assumed to be gold [30,32–35,54], with Fermi energy $E_F = 5.53$ eV and work function $W = 5.1$ eV, and the photoemission current is calculated from Eqs. (7) and (13). Since most of the electrons are emitted with initial energies near the Fermi level [10,50,55,60], for simplicity we choose the electron initial energy $\varepsilon = E_F$ for the following calculations.

In Fig. 2, we plot the photoelectron energy spectra under different dc fields with fixed gap distance $d = 5$ nm. The results for dc field $F_0 = 0$ are calculated from our recent work [54]. As shown in Fig. 2(a), adding a strong dc field $F_0 = 1$ V/nm increases the left-to-right photoelectron emission current by about 3 orders of magnitude compared to the no dc bias case $F_0 = 0$. It also shifts the dominant electron emission process from four-photon over-barrier emission ($n = 4$, cf. the ratio of the metal work function over single-photon energy $W/\hbar\omega \approx 3.29$) to dc-assisted optical tunneling emission ($n < 4$). Further increasing the dc field $F_0$ from 1 to 3 V/nm brings the dominant emission to less photon absorption (from $n = 3$ to 2). This can be explained by the fact that the potential barrier near the left metal-vacuum interface of the nanogap becomes narrower with the increase of $F_0$, enabling transition processes with fewer photons [cf. Fig. 2(b)].

However, as a larger dc field leads to a higher potential barrier at the right vacuum-metal interface of the gap, electrons in the right metal need to absorb more photons to overcome the potential barrier for emission [cf. Fig. 2(d)]. This leads to a dramatic decrease of right-to-left photoemission current and a shift of the dominant emission to

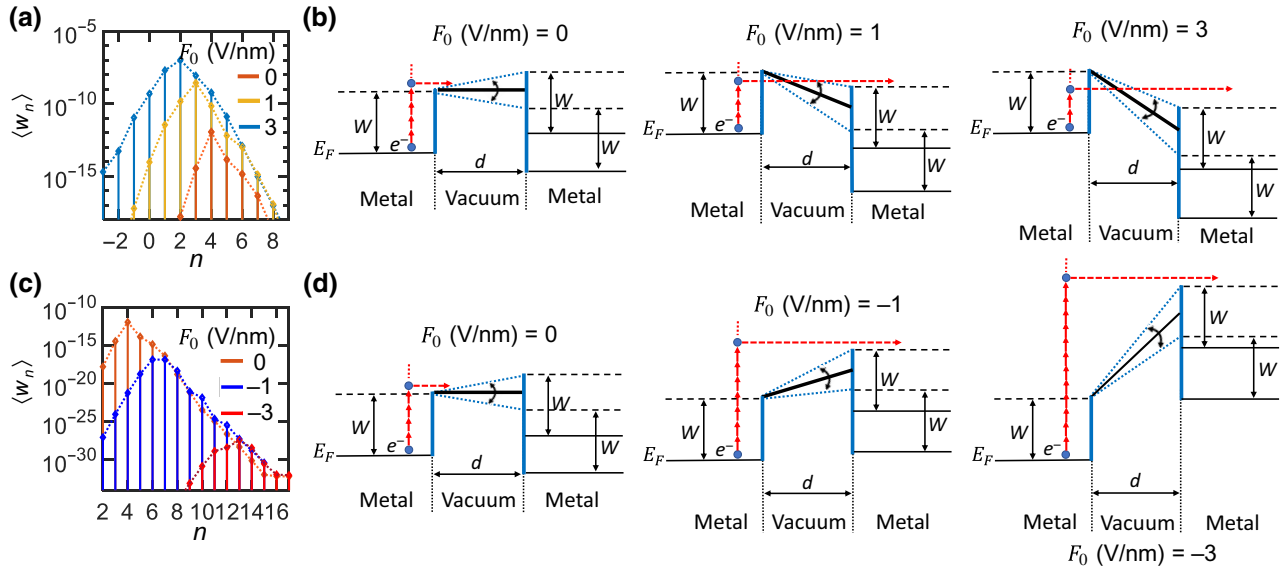


FIG. 2. (a) Photoelectron energy spectra and (b) emission mechanisms for dc field $F_0 = 0$, 1 and 3 V/nm. (c) Photoelectron energy spectra and (d) emission mechanisms for dc field $F_0 = 0$, −1 and −3 V/nm. Here, laser field $F_1$ is fixed at 1 V/nm and gap distance $d = 5$ nm.

much higher-order multiphoton absorption, as shown in Fig. 2(c).

These observed trends are also reflected in Fig. 3, which shows the total time-averaged transmission current density $\langle w \rangle$ from left- [Fig. 3(a)] and right-side [Fig. 3(b)] surfaces of the nanogap as a function of laser field $F_1$ with different applied dc bias. The increasing (decreasing) slope of the curve of $\langle w \rangle$ with dc field $F_0$ manifests the shift of main emission process to the higher- (lower-) order multiphoton absorption. Here, the slope of $\langle w \rangle$ versus $F_1$ follows the power-law scaling of photoemission $\langle w \rangle \propto F_1^{2n}$, indicating the dominant $n$-photon emission process. The value of $n$

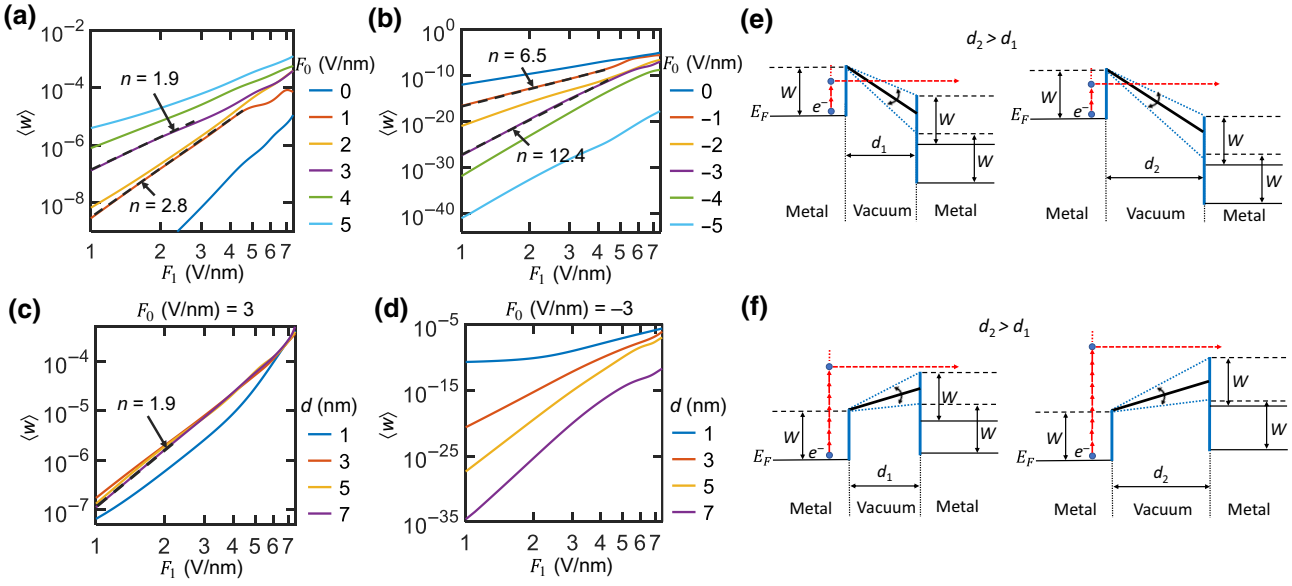


FIG. 3. Normalized total time-averaged emission current density $\langle w \rangle$ as a function of laser field $F_1$ for (a) and (b) various dc fields $F_0$ and (c) and (d) various gap distances $d$. In (a) and (b), the gap distance $d$ is fixed at 5 nm. The dashed lines denote the scaling $\langle w \rangle \propto F_1^{2n}$. $n = 2.8$, 1.9, 6.5, and 12.4 when $F_0 = 1$, 3, −1, and −3 V/nm is consistent with the observed orders of domination emission channel in Figs. 2(a) and 2(c). Emission mechanisms from the (e) left- and (f) right-side metal surface of the vacuum gap of Fig. 1(a) under the same laser electric field and dc bias for different gap distances ($d_2 > d_1$).

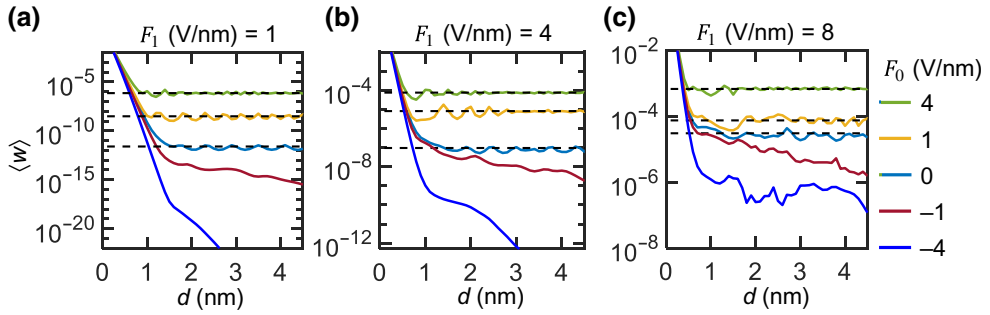


FIG. 4. Normalized total time-averaged emission current density $\langle w \rangle$ as a function of gap distance $d$ for different dc fields $F_0$ and laser fields $F_1$. Dashed lines denote the emission current density from a single surface when the right-side metal in Fig. 1(a) is removed, which is obtained from Ref. [10].

labeled in Figs. 3(a) and 3(b) is consistent with the observation in Figs. 2(a) and 2(c) (i.e., the cases with $F_0 = \pm 1$ and $\pm 3$ V/nm).

Figures 3(c) and 3(d) show the total time-averaged emission current density $\langle w \rangle$ as a function of laser field $F_1$ for different gap distances $d$ when the external dc field is fixed at 3 V/nm. For the photocurrent emitted from the left surface [Fig. 3(c)], the slope of $\langle w \rangle$ is insensitive to the gap spacing $d$ and it follows the scale $\langle w \rangle \propto F_1^{2n}$ with $n = 1.9$, indicating the dominant two-photon absorption. The insensitivity of the slope to $d$ is due to the almost unchanged potential barrier near the left metal-vacuum surface during the increase of $d$ in our model [cf. Fig. 3(e)]. It is noteworthy that, in response to changing conditions related to wave-function penetration into the barrier, in particular, the location of the barrier onset and its effective work function due to image and space charges [29,55,56,61], the potential barrier does in fact change with the gap distance $d$, which requires more careful further investigation. For the emission from the right metal surface, as $d$ increases, electrons need to absorb more photons to transport through the gap with higher potential barrier [cf. Fig. 3(f)], thus the right-to-left emission current $\langle w \rangle$ significantly decreases and its slope increases with the increasing $d$, as shown in Fig. 3(d).

In Fig. 4, we plot the total emission current density $\langle w \rangle$ as a function of gap distance $d$ under various dc fields $F_0$ and laser fields $F_1$. Without the dc bias (i.e., $F_0 = 0$), the emission current $\langle w \rangle$ from either side of the vacuum gap continuously oscillates around the current from a single surface (i.e., the dashed line) as $d$ increases. This oscillation behavior is due to the interference of electron waves inside the gap due to the reflections from the metal-vacuum interfaces, and the oscillatory behavior occurs in the multiphoton over-barrier dominant emission regime, which has been demonstrated previously [54]. After applying a large dc field (e.g., $F_0 = \pm 4$ V/nm), it is found that the oscillation in the current is greatly reduced with gap spacing $d$. This is because of the shift of main emission away from multiphoton over-barrier regime under a strong dc bias [cf. Figs. 2(a) and 2(c)], sufficiently weakening the interference effect of electron waves inside the gap.

Besides, our calculation shows with a very narrow gap ($d < 0.5$ nm), the emission current from the left and right surfaces has the same order of magnitude, regardless of applied laser intensity or dc bias, since direct tunneling dominates the electron transmission [54]. As the gap distance $d$ increases, compared to the emission current from the left metal surface, the current from the right surface is more greatly suppressed, as shown in Fig. 4, resulting in the rectified response of photoelectron emission. This indicates that varying the gap distance could provide a very different degree of rectification to the photoemission in a dc-biased vacuum gap. Our results show a gap distance of larger than 1 nm is adequate to achieve almost full rectification for dc field $F_0 \geq 1$ V/nm and laser field $F_1 \leq 8$ V/nm, and the rectification effect is more pronounced with stronger external dc bias. It is worthwhile to point out that, in practice, the externally applied field is expected to be substantially smaller than the values of the local fields noted here, because of typically strong field enhancement [27] and possible plasmonic resonant enhancement [15] near nanotips forming the gap. This may suggest a

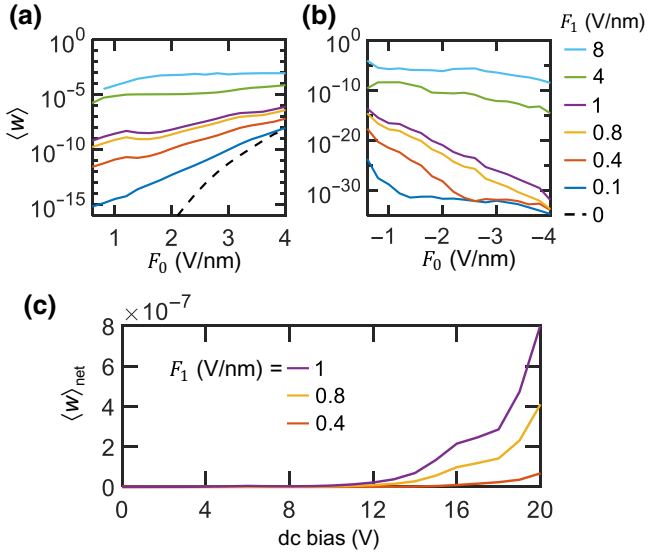


FIG. 5. (a) and (b) Normalized total time-averaged emission current density $\langle w \rangle$ as a function of dc field $F_0$ for different laser fields $F_1$. (c) Dependence of net emission current density $\langle w \rangle_{net}$, defined as the difference between the left-to-right and the right-to-left emission current density, on the applied dc bias for different laser fields $F_1$. Here, gap distance $d$ is fixed at 5 nm.

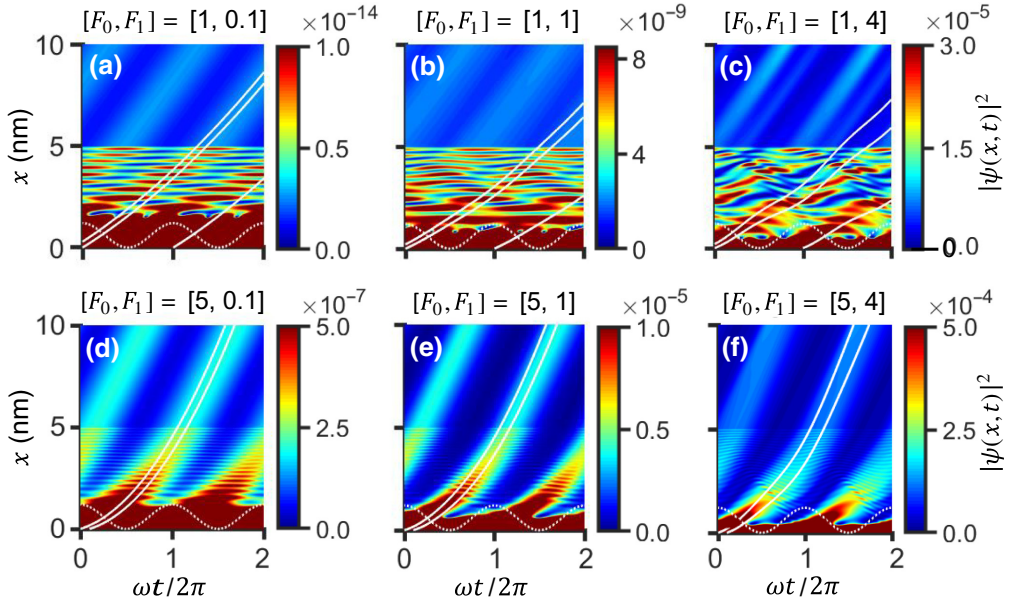


FIG. 6. Time-dependent electron density $|\psi(x,t)|^2$ from the left metal surface of the nanogap in Fig. 1(a) as a function of time $t$ and space $x$ under various combinations of dc and laser fields. Dotted white curves show the laser electric field for reference. Solid white lines represent the corresponding classical trajectories of emitted electrons, showing good agreement with the electron dynamics calculated from our model. The emission time of classical trajectory is set at around the beginning of the laser period. Here, gap distance $d$ is fixed at 5 nm. The unit of dc field $F_0$ and laser field $F_1$ is V/nm in all figures.

practical way to suppress the impact of electron signal from the direction opposite to dc field in the two-metal-tip one-way photodetection, by choosing an optimal gap spacing under a given dc bias.

In Figs. 5(a) and 5(b), we plot the total time-averaged transmission current density $\langle w \rangle$ as a function of dc field $F_0$ under different laser fields $F_1$. In Fig. 5(c), we display the net emission current density $\langle w \rangle_{\text{net}}$, defined as the difference between the left-to-right and the right-to-left emission current, as a function of external dc bias $V$ for laser field $F_1 = 0.4$, 0.8, and 1 V/nm. For zero dc bias voltage, by symmetry, emission current density from left and right metal surfaces are equal, thus no net photocurrent $\langle w \rangle_{\text{net}}$ is generated. Due to the nonlinear emission process with respect to dc field $F_0$ shown in Figs. 5(a) and 5(b), photoemission from the right surface of the gap is gradually suppressed with the increasing dc bias while that from the left increases, which leads to the rectification

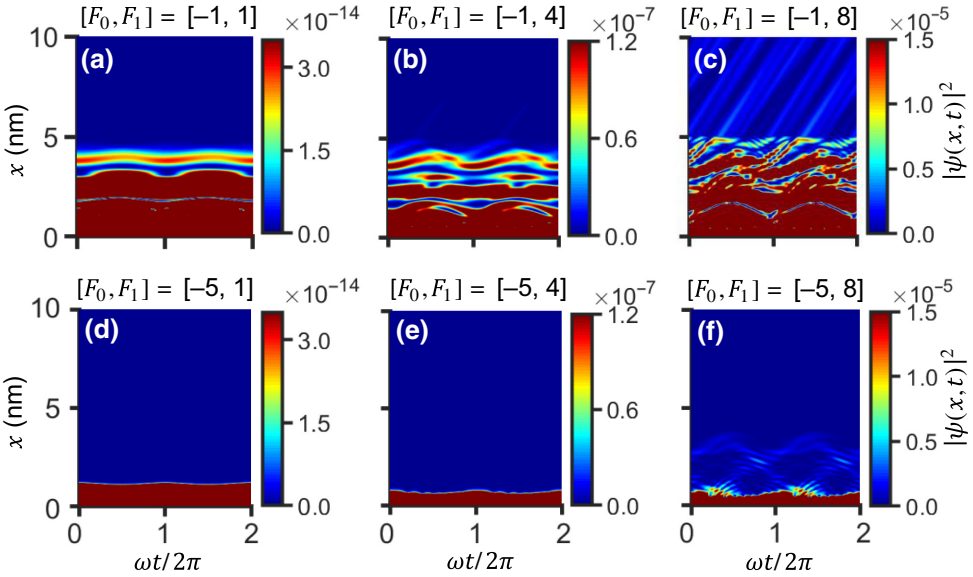


FIG. 7. Time-dependent electron density $|\psi(x,t)|^2$ from the right metal surface of the nanogap in Fig. 1(a) as a function of time $t$ and space $x$ under various combinations of dc and laser fields. Here, gap distance $d$ is fixed at 5 nm. The unit of dc field $F_0$ and laser field $F_1$ is V/nm in all figures.

response caused by applied dc bias to the photoemission [Fig. 5(c)]. The calculated increasing trend in Fig. 5(c) is in good agreement with the experimental measurement of photocurrent versus applied dc voltage in the periodic metal-vacuum nanotip array (cf. Fig. 4 in Ref. [34]).

The spatiotemporal evolution of electron density $|\psi(x,t)|^2$ emitted from left and right metal surfaces under different combinations of dc and laser electric fields is displayed in Figs. 6 and 7, respectively. Here, the gap distance $d$ is fixed at 5 nm. As seen in Fig. 6(a), with a larger applied dc field $F_0 = 1$ V/nm and a weaker laser field $F_1 = 0.1$ V/nm, parts of electrons emitted from the left metal surface are reflected back and forth inside the gap ($0 < x < 5$ nm). These emission patterns are in line with the numerical simulation results in Fig. 2(a) of Ref. [38]. Increasing the laser field $F_1$ in Figs. 6(a)–6(c) is found to produce stronger oscillatory features within the gap. It is due to the stronger backpropagation and acceleration processes (i.e., quiver motion) of emitted electrons under strong laser electric fields [16]. When adding a stronger dc field $F_0 = 5$ V/nm, dc-fieldlike electron emission pattern dominates the whole regime, as shown in Figs. 6(d)–6(f). Due to the strong acceleration, electrons enter the right-side metal with higher velocity compared to the case with $F_0 = 1$ V/nm (cf. the slope of white solid lines representing classical emission trajectories). On the other hand, for the emission from the right surface, as seen in Fig. 7, the addition of 1 V/nm dc field confines most of the electrons inside the vacuum gap, and only when the laser field $F_1$ is increased up to 8 V/nm could a small part of electrons escape from the gap into left metal [Fig. 7(c)]. A similar trend can be observed in Figs. 7(d)–7(f) when applying a larger dc field of 5 V/nm, where most of the electrons are constrained in the strong surface current oscillation regime.

## IV. CONCLUSION

In summary, by exactly solving the time-dependent Schrödinger equation, we present an analytical model for nonlinear photoelectron emission from a dc-biased nanoscale metal-vacuum-metal gap driven by a laser field. Our results reveal the underlying photoemission processes, time-averaged emission current and spatiotemporal dynamics of photoelectrons from left- and right-side surfaces of the nanogap under different combinations of dc bias, laser fields and gap distances. Our calculation shows that applying a strong dc bias can greatly reduce the interference oscillation in the single-sided transmission current, due to the shift of dominant emission away from multiphoton over-barrier regime. We demonstrate that in addition to the dc bias, varying the gap spacing can greatly influence the rectification to the photoelectron emission in a dc-biased vacuum gap. This may provide guidance to suppress the impact of electron signal from the direction opposite to dc field on the one-way photodetection by choosing proper gap spacing with a given dc bias. Our work would be helpful for understanding the photoemission properties in dc-biased asymmetric metal-vacuum nanojunctions, and for the design of advanced quantum plasmonic nanoantennas and ultrafast photodetectors. Future work will consider the effects of ultrashort pulsed laser illumination [16], laser penetration depth, laser heating [62], space charge [29,55,56], oscillatory Schottky barrier lowering [29,55,56,61], dielectric surface coating [15,63,64], roughness and defects, asymmetric geometry [27], and dissimilar electrode materials [56] on photoemission in a nanogap.

## ACKNOWLEDGMENTS

This work is supported by Air Force Office of Scientific Research (AFOSR) YIP Grant (No. FA9550-18-1-0061) and Office of Naval Research (ONR) YIP Grant (No. N00014-20-1-2681).

## APPENDIX A: EXACT SOLUTION OF ELECTRON WAVE FUNCTION

Following Truscott [10,65], the time-dependent potential energy for $0 \le x < d$ can be written as $\Phi(x,t) = V(x,t) - xf(t)$. Thus, the TDSE [Eq. (2)] can be transformed to the coordinate system $\xi$, $t$, where $\xi = x - q(t)$, the displacement $q(t) = (1/m_e)\int^t p(t')dt'$, and $p(t) = \int^t f(t')dt'$, by assuming that $\psi(x,t) = \phi(\xi,t)\chi(x,t)$, with $\chi(x,t) = \exp\left[-iEt/\hbar + ixp(t)/\hbar - (i/2\hbar m_e)\int^t p^2(t')dt'\right]$, and $E$ being a constant. Then, we have

$$i\hbar\frac{\partial\phi(\xi,t)}{\partial t} = \left[-\frac{\hbar^2}{2m_e}\frac{\partial^2}{\partial\xi^2} + U(\xi,t) - E\right]\phi(\xi,t), \quad \text{(A1)}$$

with $U(\xi,t) = V(x,t)$. By separation of variables, $\phi(\xi,t)$ in Eq. (A1) can be solved. From $\psi(x,t) = \phi(\xi,t)\chi(x,t)$, we obtain exact solution of electron wave function.

For photoelectron emission from the left metal-vacuum interface of the gap in Fig. 1(a), we have the potential energy $\Phi(x,t) = V(x) - xf(t)$, with $V(x,t) = V_0 - eVx/d$ where $V_0 = E_F + W$ and $f(t) = eF_1\cos(\omega t)$ [cf. Eq. (1)], and

$$\phi(\xi,t) = g(\xi)\exp\left[\frac{e^2VF_1\sin(\omega t)}{i\hbar d m_e\omega^3}\right], \quad \text{(A2)}$$

where $g(\xi) = \mathrm{Ai}(-\eta) \pm i\mathrm{Bi}(-\eta)$ is the solution of the equation $-(\hbar^2/2m_e)\partial^2 g(\xi)/\partial\xi^2 + (V_0 - E - eV\xi/d)g(\xi) = 0$, where $\eta = (2em_eV/d\hbar^2)^{1/3}[(E - V_0)d/eV + \xi]$ [10,57]. Here, "−" in $g(\xi)$ denotes the electron wave traveling towards $+x$ direction; "+" denotes the electron wave traveling towards $-x$ direction. Due to the reflection of electron waves at metal-vacuum surfaces of $x = 0$ and $d$ [cf. Fig. 1(b)], the electron wave function $\psi(x,t)$ inside the vacuum gap ($0 \le x < d$) should be the superposition

of wave functions towards $+x$ direction and $-x$ direction. Then, from $\psi(x,t) = \phi(\xi,t)\chi(x,t)$, we obtain Eq. (4) with $E = \varepsilon + n\hbar\omega - e^2F_1^2/4m_e\omega^2$.

For the photoelectron emission from the right vacuum-metal interface of the gap in Fig. 1(a), we have the potential energy $\Phi(x,t) = V(x) - xf(t)$, with $V(x,t) = V_0 + eVx/d$ where $V_0 = E_F + W$ and $f(t) = eF_1\cos(\omega t)$ [cf. Eq. (8)], and

$$\phi(\xi,t) = g(\xi)\exp\left[-\frac{e^2VF_1\sin(\omega t)}{i\hbar dm_e\omega^3}\right], \tag{A3}$$

where $g(\xi) = \mathrm{Ai}(\eta) \pm i\mathrm{Bi}(\eta)$ is the solution of the equation $-(\hbar^2/2m_e)\partial^2 g(\xi)/\partial\xi^2 + (V_0 - E + eV\xi/d)g(\xi) = 0$, where $\eta = (2em_eV/d\hbar^2)^{1/3}[\xi - (E - V_0)d/eV]$ [10,57]. Here, "+" in $g(\xi)$ denotes the electron wave traveling towards $+x$ direction; "−" denotes the electron wave traveling towards $-x$ direction. Due to the reflection of electron waves at metal-vacuum surfaces of $x = 0$ and $d$ [cf. Fig. 1(c)], the electron wave function $\psi(x,t)$ inside the vacuum gap ($0 \le x < d$) should be the superposition of wave functions towards $+x$ direction and $-x$ direction. Then, from $\psi(x,t) = \phi(\xi,t)\chi(x,t)$, we obtain Eq. (10) with $E = \varepsilon + n\hbar\omega - e^2F_1^2/4m_e\omega^2$.

## APPENDIX B: CALCULATION OF TRANSMISSION AND REFLECTION COEFFICIENTS

For the photoemission from the left metal-vacuum interface of the gap in Fig. 1(a), by applying the boundary conditions that both the electron wave function $\psi(x,t)$ and its derivative $\partial\psi(x,t)/\partial x$ are continuous at $x = 0$ and $x = d$ [cf. Fig. 1(b)], and taking Fourier transform, we obtain, in nondimensional quantities, $\bar{\varepsilon} = \varepsilon/W$, $\bar{\omega} = \omega\hbar/W$, $\bar{t} = tW/\hbar$, $\bar{E}_F = E_F/W$, $\bar{x} = x/\lambda_0$, $\bar{d} = d/\lambda_0$, $\lambda_0 = \sqrt{\hbar^2/2m_eW}$, $\bar{V} = Ve/W$, $\bar{F}_1 = F_1e\lambda_0/W$, $\bar{U}_p = U_p/W$, the following equations:

$$\sum_{n=-\infty}^{\infty} T_{1n}\left[\sqrt{\bar{\varepsilon} + m\bar{\omega}}P_{1n(n-m)} + Q_{1n(n-m)}\right] + T_{2n}[\sqrt{\bar{\varepsilon} + m\bar{\omega}}P_{2n(n-m)} + Q_{2n(n-m)}] = 2\sqrt{\bar{\varepsilon}}\delta(m), \tag{B1}$$

$$\sum_{n=-\infty}^{\infty}\left[\sqrt{\bar{\varepsilon} + m\bar{\omega} + \bar{V}}U_{1n(n-m)} - V_{1n(n-m)}\right]T_{1n} + \left[\sqrt{\bar{\varepsilon} + m\bar{\omega} + \bar{V}}U_{2n(n-m)} - V_{2n(n-m)}\right]T_{2n} = 0, \tag{B2}$$

$$\sum_{n=-\infty}^{\infty} T_{1n}U_{1n(n-m)} + T_{2n}U_{2n(n-m)} = T_{3m}\exp\left(i\bar{d}\sqrt{\bar{\varepsilon} + m\bar{\omega} + \bar{V}}\right), \tag{B3}$$

where $\delta(m)$, $P_{1n(n-m)}$, $Q_{1n(n-m)}$, $P_{2n(n-m)}$, $Q_{2n(n-m)}$, $U_{1n(n-m)}$, $V_{1n(n-l)}$, $U_{2n(n-m)}$, and $V_{2n(n-l)}$ are given by

$$\delta(m) = \begin{cases} 1, & m = 0, \\ 0, & m \neq 0, \end{cases} \tag{B4a}$$

$$P_{1nl} = \frac{1}{2\pi}\int_0^{2\pi} p_{1n}(\bar{\omega}\bar{t})e^{-il\bar{\omega}\bar{t}}d(\bar{\omega}\bar{t}),$$

$$Q_{1nl} = \frac{1}{2\pi}\int_0^{2\pi} q_{1n}(\bar{\omega}\bar{t})e^{-il\bar{\omega}\bar{t}}d(\bar{\omega}\bar{t}), \tag{B4b}$$

$$P_{2nl} = \frac{1}{2\pi}\int_0^{2\pi} p_{2n}(\bar{\omega}\bar{t})e^{-il\bar{\omega}\bar{t}}d(\bar{\omega}\bar{t}),$$

$$Q_{2nl} = \frac{1}{2\pi}\int_0^{2\pi} q_{2n}(\bar{\omega}\bar{t})e^{-il\bar{\omega}\bar{t}}d(\bar{\omega}\bar{t}), \tag{B4c}$$

$$p_{1n}(\bar{\omega}\bar{t}) = \mathrm{Ai}(\alpha_n)f(\bar{\omega}\bar{t}), \tag{B4d}$$

$$q_{1n}(\bar{\omega}\bar{t}) = \left[\mathrm{Ai}(\alpha_n)\frac{\bar{F}_1\sin(\bar{\omega}\bar{t})}{\bar{\omega}} + i\mathrm{Ai}'(\alpha_n)\left(\frac{\bar{V}}{\bar{d}}\right)^{\frac{1}{3}}\right]f(\bar{\omega}\bar{t}), \tag{B4e}$$

$$p_{2n}(\bar{\omega}\bar{t}) = \mathrm{Bi}(\alpha_n)f(\bar{\omega}\bar{t}), \tag{B4f}$$

$$q_{2n}(\bar{\omega}\bar{t}) = \left[\mathrm{Bi}(\alpha_n)\frac{\bar{F}_1\sin(\bar{\omega}\bar{t})}{\bar{\omega}} + i\mathrm{Bi}'(\alpha_n)\left(\frac{\bar{V}}{\bar{d}}\right)^{\frac{1}{3}}\right]f(\bar{\omega}\bar{t}), \tag{B4g}$$

$$U_{1nl} = \frac{1}{2\pi}\int_0^{2\pi} u_{1n}(\bar{\omega}\bar{t})e^{-il\bar{\omega}\bar{t}}d(\bar{\omega}\bar{t}),$$

$$V_{1nl} = \frac{1}{2\pi}\int_0^{2\pi} v_{1n}(\bar{\omega}\bar{t})e^{-il\bar{\omega}\bar{t}}d(\bar{\omega}\bar{t}), \tag{B4h}$$

$$U_{2nl} = \frac{1}{2\pi}\int_0^{2\pi} u_{2n}(\bar{\omega}\bar{t})e^{-il\bar{\omega}\bar{t}}d(\bar{\omega}\bar{t}),$$

$$V_{2nl} = \frac{1}{2\pi}\int_0^{2\pi} v_{2n}(\bar{\omega}\bar{t})e^{-il\bar{\omega}\bar{t}}d(\bar{\omega}\bar{t}), \tag{B4i}$$

$$u_{1n}(\bar{\omega}\bar{t}) = Ai(\gamma_n)f(\bar{\omega}\bar{t}), \tag{B4j}$$

$$v_{1n}(\bar{\omega}\bar{t}) = \left[\mathrm{Ai}(\gamma_n)\frac{\bar{F}_1\sin(\bar{\omega}\bar{t})}{\bar{\omega}} + i\mathrm{Ai}'(\gamma_n)\left(\frac{\bar{V}}{\bar{d}}\right)^{\frac{1}{3}}\right]f(\bar{\omega}\bar{t}), \tag{B4k}$$

$$u_{2n}(\bar{\omega}\bar{t}) = \mathrm{Bi}(\gamma_n)f(\bar{\omega}\bar{t}), \tag{B4l}$$

$$v_{2n}(\bar{\omega}\bar{t}) = \left[\mathrm{Bi}(\gamma_n)\frac{\bar{F}_1\sin(\bar{\omega}\bar{t})}{\bar{\omega}} + i\mathrm{Bi}'(\gamma_n)\left(\frac{\bar{V}}{\bar{d}}\right)^{\frac{1}{3}}\right]f(\bar{\omega}\bar{t}), \tag{B4m}$$

$$f(\bar{\omega}\bar{t}) = \exp\left[-i\frac{2\bar{F}_1\bar{V}}{\bar{d}\bar{\omega}^3}\sin(\bar{\omega}\bar{t}) + i\frac{\bar{F}_1^2}{4\bar{\omega}^3}\sin(2\bar{\omega}\bar{t})\right], \tag{B4n}$$

with $\alpha_n = -[\bar{E}_n\bar{d}/\bar{V} + 2\bar{F}_1\cos(\bar{\omega}\bar{t})/\bar{\omega}^2](\bar{V}/\bar{d})^{1/3}$, $\gamma_n = -[\bar{E}_n\bar{d}/\bar{V} + \bar{d} + 2\bar{F}_1\cos(\bar{\omega}\bar{t})/\bar{\omega}^2](\bar{V}/\bar{d})^{1/3}$, and $\bar{E}_n = \bar{\varepsilon} + n\bar{\omega} - \bar{E}_F - \bar{U}_p - 1$. The coefficients $T_{1n}$, $T_{2n}$, and $T_{3n}$ (and therefore $R_{1n}$) is then calculated from Eqs. (B1)–(B3).

For the photoemission from the right vacuum-metal interface of the gap in Fig. 1(a), applying the boundary conditions yields the almost same equations as the case from the left metal surface above, except that "$\bar{V}$" in Eqs. (B2), (B3), and (B4n) is replaced by "$-\bar{V}$", "+" in Eqs. (B4e), (B4g), (B4k), and (B4m) is replaced by "−", $\alpha_n = [2\bar{F}_1\cos(\bar{\omega}\bar{t})/\bar{\omega}^2 - \bar{E}_n\bar{d}/\bar{V}](\bar{V}/\bar{d})^{1/3}$, and $\gamma_n = [\bar{d} + 2\bar{F}_1\cos(\bar{\omega}\bar{t})/\bar{\omega}^2 - \bar{E}_n\bar{d}/\bar{V}](\bar{V}/\bar{d})^{1/3}$.


[1] P. Hommelhoff, C. Kealhofer, and M. A. Kasevich, Ultrafast Electron Pulses From a Tungsten Tip Triggered by Low-Power Femtosecond Laser Pulses, Phys. Rev. Lett. **97**, 247402 (2006).

[2] C. Ropers, D. R. Solli, C. P. Schulz, C. Lienau, and T. Elsaesser, Localized Multiphoton Emission of Femtosecond Electron Pulses From Metal Nanotips, Phys. Rev. Lett. **98**, 043907 (2007).

[3] R. Bormann, M. Gulde, A. Weismann, S. V. Yalunin, and C. Ropers, Tip-Enhanced Strong-Field Photoemission, Phys. Rev. Lett. **105**, 147601 (2010).

[4] M. Schenk, M. Krüger, and P. Hommelhoff, Strong-field Above-Threshold Photoemission From Sharp Metal Tips, Phys. Rev. Lett. **105**, 257601 (2010).

[5] M. Krüger, M. Schenk, and P. Hommelhoff, Attosecond control of electrons emitted from a nanoscale metal Tip, Nature **475**, 78 (2011).

[6] P. Dombi, A. Hörl, P. Rácz, I. Márton, A. Trügler, J. R. Krenn, and U. Hohenester, Ultrafast strong-field photoemission from plasmonic nanoparticles, Nano Lett. **13**, 674 (2013).

[7] R. G. Hobbs, Y. Yang, A. Fallahi, P. D. Keathley, E. De Leo, F. X. Kärtner, W. S. Graves, and K. K. Berggren, High-yield, ultrafast, surface plasmon-enhanced, Au nanorod optical field electron emitter arrays, ACS Nano **8**, 11474 (2014).

[8] M. E. Swanwick, P. D. Keathley, A. Fallahi, P. R. Krogen, G. Laurent, J. Moses, F. X. Kärtner, and L. F. Velásquez-García, Nanostructured ultrafast silicon-tip optical field-emitter arrays, Nano Lett. **14**, 5035 (2014).

[9] L. Wimmer, G. Herink, D. R. Solli, S. V. Yalunin, K. E. Echternkamp, and C. Ropers, Terahertz control of nanotip photoemission, Nat. Phys. **10**, 432 (2014).

[10] P. Zhang and Y. Y. Lau, Ultrafast strong-field photoelectron emission from biased metal surfaces: Exact solution to time-dependent schrödinger equation, Sci. Rep. **6**, 19894 (2016).

[11] W. P. Putnam, R. G. Hobbs, P. D. Keathley, K. K. Berggren, and F. X. Kärtner, Optical-field-controlled photoemission from plasmonic nanoparticles, Nat. Phys. **13**, 335 (2017).

[12] Y. Luo and P. Zhang, Ultrafast strong-field photoelectron emission due to two-color laser fields, Phys. Rev. B **98**, 165442 (2018).

[13] M. Sivis, N. Pazos-Perez, R. Yu, R. Alvarez-Puebla, F. J, García de Abajo, and C. Ropers, Continuous-wave multiphoton photoemission from plasmonic nanostars, Commun. Phys. **1**, 1 (2018).

[14] M. Reutzel, A. Li, and H. Petek, Coherent two-Dimensional Multiphoton Photoelectron Spectroscopy of Metal Surfaces, Phys. Rev. X **9**, 011044 (2019).

[15] X. Xiong, Y. Zhou, Y. Luo, X. Li, M. Bosman, L. K. Ang, P. Zhang, and L. Wu, Plasmon-enhanced resonant photoemission using atomically thick dielectric coatings, ACS Nano **14**, 8806 (2020).

[16] Y. Luo, Y. Zhou, and P. Zhang, Few-cycle optical-field-induced photoemission from biased surfaces: An exact quantum theory, Phys. Rev. B **103**, 085410 (2021).

[17] M. Müller, A. Paarmann, and R. Ernstorfer, Femtosecond electrons probing currents and atomic structure in nanomaterials, Nat. Commun. **5**, 5292 (2014).

[18] A. Feist, N. Bach, N. Rubiano da Silva, T. Danz, M. Möller, K. E. Priebe, T. Domröse, J. G. Gatzmann, S. Rost, J. Schauss, S. Strauch, R. Bormann, M. Sivis, S. Schäfer, and C. Ropers, Ultrafast transmission electron microscopy using a laser-driven field emitter: Femtosecond resolution with a high coherence electron beam, Ultramicroscopy **176**, 63 (2017).

[19] S. Sun, X. Sun, D. Bartles, E. Wozniak, J. Williams, P. Zhang, and C.-Y. Ruan, Direct imaging of plasma waves using ultrafast electron microscopy, Struct. Dyn. **7**, 064301 (2020).

[20] K. Yoshioka, I. Katayama, Y. Minami, M. Kitajima, S. Yoshida, H. Shigekawa, and J. Takeda, Real-space coherent manipulation of electrons in a single tunnel junction by single-cycle terahertz electric fields, Nat. Photonics **10**, 762 (2016).

[21] D. Ehberger, J. Hammer, M. Eisele, M. Krüger, J. Noe, A. Högele, and P. Hommelhoff, Highly Coherent Electron Beam From a Laser-Triggered Tungsten Needle Tip, Phys. Rev. Lett. **114**, 227601 (2015).

[22] B. Schröder, M. Sivis, R. Bormann, S. Schäfer, and C. Ropers, An ultrafast nanotip electron Gun triggered by grating-coupled surface plasmons, Appl. Phys. Lett. **107**, 231105 (2015).

[23] E. Jones, M. Becker, J. Luiten, and H. Batelaan, Laser control of electron matter waves, Laser Photonics Rev. **10**, 214 (2016).

[24] R. J. England, *et al.*, Dielectric laser accelerators, Rev. Mod. Phys. **86**, 1337 (2014).

[25] E. Forati, T. J. Dill, A. R. Tao, and D. Sievenpiper, Photoemission-Based microelectronic devices, Nat. Commun. **7**, 13399 (2016).

[26] P. Zhang and Y. Y. Lau, Ultrafast and nanoscale diodes, J. Plasma Phys. **82**, 595820505 (2016).

[27] J. Lin, P. Y. Wong, P. Yang, Y. Y. Lau, W. Tang, and P. Zhang, Electric field distribution and current emission in a miniaturized geometrical diode, J. Appl. Phys. **121**, 244301 (2017).

[28] P. Zhang, Á Valfells, L. K. Ang, J. W. Luginsland, and Y. Y. Lau, 100 years of the physics of diodes, Appl. Phys. Rev. **4**, 011304 (2017).

[29] P. Zhang, Y. S. Ang, A. L. Garner, Á Valfells, J. W. Luginsland, and L. K. Ang, Space–charge limited current in

nanodiodes: Ballistic, collisional, and dynamical effects, J. Appl. Phys. **129**, 100902 (2021).
[30] D. R. Ward, F. Hüser, F. Pauly, J. C. Cuevas, and D. Natelson, Optical rectification and field enhancement in a plasmonic nanogap, Nat. Nanotechnol. **5**, 732 (2010).
[31] T. Higuchi, L. Maisenbacher, A. Liehl, P. Dombi, and P. Hommelhoff, A nanoscale vacuum-tube diode triggered by Few-cycle laser pulses, Appl. Phys. Lett. **106**, 051109 (2015).
[32] T. Rybka, M. Ludwig, M. F. Schmalz, V. Knittel, D. Brida, and A. Leitenstorfer, Sub-cycle optical phase control of nanotunnelling in the single-electron regime, Nat. Photonics **10**, 667 (2016).
[33] P. Rácz, Z. Pápa, I. Márton, J. Budai, P. Wróbel, T. Stefaniuk, C. Prietl, J. R. Krenn, and P. Dombi, Measurement of nanoplasmonic field enhancement with ultrafast photoemission, Nano Lett. **17**, 1181 (2017).
[34] S. Piltan and D. Sievenpiper, Plasmonic nano-arrays for enhanced photoemission and photodetection, J. Opt. Soc. Am. B **35**, 208 (2018).
[35] J. Heimerl, T. Higuchi, M. Ammon, M. A. Schneider, and P. Hommelhoff, Gap-size dependence of optical near fields in a variable nanoscale two-tip junction, Phys. Rev. B **101**, 125403 (2020).
[36] M. Ludwig, G. Aguirregabiria, F. Ritzkowsky, T. Rybka, D. C. Marinica, J. Aizpurua, A. G. Borisov, A. Leitenstorfer, and D. Brida, Sub-femtosecond electron transport in a nanoscale Gap, Nat. Phys. **16**, 341 (2020).
[37] M. Ludwig, A. K. Kazansky, G. Aguirregabiria, D. C. Marinica, M. Falk, A. Leitenstorfer, D. Brida, J. Aizpurua, and A. G. Borisov, Active control of ultrafast electron dynamics in plasmonic gaps using an applied bias, Phys. Rev. B **101**, 241412 (2020).
[38] M. Turchetti, M. R. Bionta, Y. Yang, F. Ritzkowsky, F. Ritzkowsky, D. R. Candido, M. E. Flatté, K. K. Berggren, and P. D. Keathley, Impact of DC bias on weak optical-field-driven electron emission in nano-vacuum-gap detectors, J. Opt. Soc. Am. B **38**, 1009 (2021).
[39] L. V. Keldysh, Ionization in the field of a strong electromagnetic wave, J. Exp. Theor. Phys. **20**, 1307 (1965).
[40] C. Caroli, R. Combescot, D. Lederer, P. Nozieres, and D. Saint-James, A direct calculation of the tunnelling current. II. Free electron description, J. Phys. C: Solid State Phys. **4**, 2598 (1971).
[41] F. H. M. Faisal, Multiple absorption of laser photons by atoms, J. Phys. B: Atom. Mol. Phys. **6**, L89 (1973).
[42] H. D. Jones and H. R. Reiss, Intense-field effects in solids, Phys. Rev. B **16**, 2466 (1977).
[43] H. R. Reiss, Effect of an intense electromagnetic field on a weakly bound system, Phys. Rev. A **22**, 1786 (1980).
[44] H. R. Reiss, Complete Keldysh theory and its limiting cases, Phys. Rev. A **42**, 1476 (1990).
[45] F. H. M. Faisal and J. Z. Kamiński, Floquet-Bloch theory of high-harmonic generation in periodic structures, Phys. Rev. A **56**, 748 (1997).
[46] L. B. Madsen, Gauge invariance in the interaction between atoms and few-cycle laser pulses, Phys. Rev. A **65**, 053417 (2002).
[47] F. H. M. Faisal, J. Z. Kamiński, and E. Saczuk, Photoemission and high-order harmonic generation from solid surfaces in intense laser fields, Phys. Rev. A **72**, 023412 (2005).
[48] L. B. Madsen, Strong-field approximation in laser-assisted dynamics, Am. J. Phys. **73**, 57 (2005).
[49] L. V. Keldysh, Multiphoton ionization by a very short pulse, Phys.-Usp. **60**, 1187 (2017).
[50] S. V. Yalunin, M. Gulde, and C. Ropers, Strong-field photoemission from surfaces: Theoretical approaches, Phys. Rev. B **84**, 195426 (2011).
[51] D. C. Marinica, A. K. Kazansky, P. Nordlander, J. Aizpurua, and A. G. Borisov, Quantum plasmonics: Nonlinear effects in the field enhancement of a plasmonic nanoparticle dimer, Nano Lett. **12**, 1333 (2012).
[52] W. Zhu, R. Esteban, A. G. Borisov, J. J. Baumberg, P. Nordlander, H. J. Lezec, J. Aizpurua, and K. B. Crozier, Quantum mechanical effects in plasmonic structures with subnanometre gaps, Nat. Commun. **7**, 11495 (2016).
[53] L. Wu, H. Duan, P. Bai, M. Bosman, J. K. W. Yang, and E. Li, Fowler–nordheim tunneling induced charge transfer plasmons between nearly touching nanoparticles, ACS Nano **7**, 707 (2013).
[54] Y. Luo and P. Zhang, Ultrafast optical-field-induced photoelectron emission in a vacuum nanoscale Gap: An exact analytical formulation, Appl. Phys. Lett. **119**, 194101 (2021).
[55] P. Zhang, Scaling for quantum tunneling current in nano- and subnano-scale plasmonic junctions, Sci. Rep. **5**, 9826 (2015).
[56] S. Banerjee and P. Zhang, A generalized self-consistent model for quantum tunneling current in dissimilar metal-insulator-metal junction, AIP Adv. **9**, 085302 (2019).
[57] Y. Luo and P. Zhang, Analysis of two-Color Laser-Induced Electron Emission From a Biased Metal Surface Using an Exact Quantum Mechanical Solution, Phys. Rev. Appl. **12**, 044056 (2019).
[58] Y. Luo, J. Luginsland, and P. Zhang, Interference modulation of photoemission from biased metal cathodes driven by two lasers of the same frequency, AIP Adv. **10**, 075301 (2020).
[59] Y. Zhou and P. Zhang, A quantum model for photoemission from metal surfaces and Its comparison with the three-step model and Fowler–DuBridge model, J. Appl. Phys. **127**, 164903 (2020).
[60] J. W. Gadzuk and E. W. Plummer, Field emission energy distribution (FEED), Rev. Mod. Phys. **45**, 487 (1973).
[61] R. G. Forbes, The electrical surface as centroid of the surface-induced charge, Ultramicroscopy **79**, 25 (1999).
[62] Y. Zhou and P. Zhang, Quantum efficiency of photoemission from biased metal surfaces with laser wavelengths from UV to NIR, J. Appl. Phys. **130**, 064902 (2021).
[63] Y. Zhou and P. Zhang, Theory of field emission from dielectric coated surfaces, Phys. Rev. Res. **2**, 043439 (2020).
[64] Y. Zhou and P. Zhang, Theory of laser-induced photoemission from a metal surface with nanoscale dielectric coating, J. Appl. Phys. **131**, 064903 (2022).
[65] W. S. Truscott, Wave Functions in the Presence of a Time-Dependent Field: Exact Solutions and Their Application to Tunneling, Phys. Rev. Lett. **70**, 1900 (1993).